Simulating the response of terahertz radiation to basal cell carcinoma using *ex vivo* spectroscopy measurements

Emma Pickwell
Cambridge University
Cavendish Laboratory
Semiconductor Physics Group
Madingley Road
Cambridge CB3 0HE
United Kingdom
and
TeraView Limited
Platinum Building
St. John's Innovation Park
Cambridge CB4 0WS
United Kingdom

Anthony J. Fitzgerald
Bryan E. Cole
Philip F. Taday
TeraView, Limited
Platinum Building
St. John's Innovation Park
Cambridge CB4 0WS
United Kingdom

Richard J. Pye
Thomas Ha
Addenbrooke's Hospital
Department of Dermatology
Cambridge CB2 2QQ
United Kingdom

Michael Pepper
Cambridge University
Cavendish Laboratory
Semiconductor Physics Group
Madingley Road
Cambridge CB3 0HE
United Kingdom
and
TeraView Limited
Platinum Building
St. John's Innovation Park
Cambridge CB4 0WS
United Kingdom

Vincent P. Wallace
TeraView, Limited
Platinum Building
St. John's Innovation Park
Cambridge CB4 0WS
United Kingdom

Abstract. Studies of basal cell carcinoma using terahertz pulsed imaging have revealed a significant difference between regions of tumor and healthy tissue. These differences are manifested in the reflected pulse due to what is thought to be changes in refractive index and absorption. We present measurements of the refractive index and absorption coefficient of excised normal tissue and basal cell carcinoma using terahertz (THz) transmission spectroscopy. We extract Debye parameters from these data and enter them into a finite difference time domain simulation to predict the shape of the waveforms reflected off the normal tissue and basal cell carcinoma and compare them with published *in vivo* data. Simulating the interaction of terahertz radiation with normal and cancerous tissue is a key step toward understanding the origin of contrast in terahertz images of skin cancer.
 [DOI: 10.1117/1.2137667]

Keywords: modeling; finite difference time domain; cancer; terahertz imaging; terahertz pulsed imaging.

Paper 05028R received Feb. 2, 2005; revised manuscript received Jun. 10, 2005; accepted for publication Jun. 27, 2005; published online Dec. 8, 2005.

1 Introduction

Terahertz Pulsed Imaging (TPI T) is a novel, noninvasive, imaging modality with current applications in pharmaceuticals,[1] security,[2] and medicine.[3] TPI uses pulses of electromagnetic radiation typically with a full width half maximum of 0.3 picosec and an average power of 100 nW. The pulses are detected coherently using a photoconductive device, and the Fourier transformed pulse gives a usable frequency range of 0.1 to 4 THz.[4] These frequencies typically

Address all correspondence to Emma Pickwell, TeraView Ltd., Platinum Building — St. John's Innovation Park, Cambridge, CB4 0WS United Kingdom. Tel: +44 (0) 1223 435 380. Fax: +44 (0) 1223 435 382. E-mail: emma.pickwell@teraview.com

1083-3668/2005/10(6)/064021/7/$22.00 © 2005 SPIE

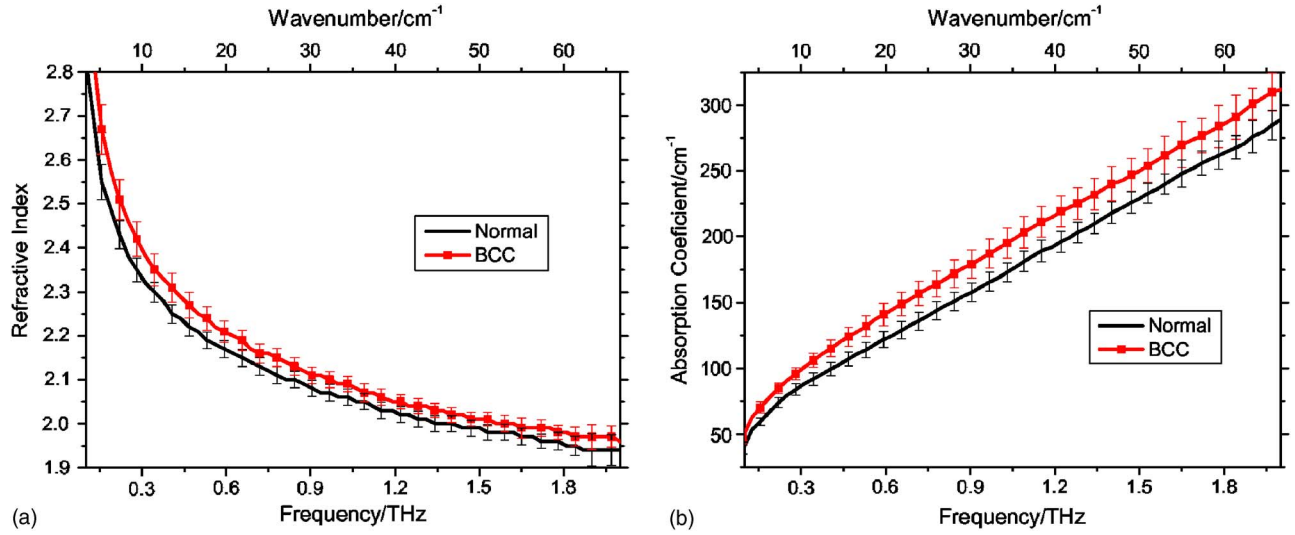

Fig. 1 (a) The refractive index and (b) the absorption coefficient of normal tissue and that containing BCC. The error bars represent 95% confidence limits.

interact with lattice vibrations of crystalline substances and hydrogen bonds in liquids, thus making TPI extremely sensitive to water content in tissues. Terahertz (THz) radiation is nonionizing, and power levels used for this study are well within safety guidelines.[5]

It has been shown using TPI that there is a significant difference between the response of terahertz radiation to basal cell carcinoma (BCC) compared to normal skin.[6,7] Evidence from PET and MRI studies indicates that tumors have increased water content.[8–11] Therefore, as water has strong absorptions across the entire terahertz range,[12] it is likely that changes in water content are a main source of image contrast. We have previously modeled the interaction of terahertz radiation with water[13] and *in vivo* skin[14] to investigate the source of image contrast.

In this work, we use terahertz spectroscopy measurements of normal skin and basal cell carcinoma (BCC) to investigate the differences in their refractive indices and absorption coefficients in the terahertz regime. We fit the measured properties to double Debye theory[15] and use finite difference time domain (FDTD) methods to simulate the interaction of terahertz radiation with normal skin and BCC. We investigate how the double Debye parameters determine the shape of the waveforms reflected off BCCs. In addition, we use the model to simulate waveforms to fit *in vivo* terahertz data of skin cancer. Finally, we compare the differences between terahertz properties measured *ex vivo* with those differences between terahertz properties of normal and diseased tissue extracted from the image simulation.

This work has wide ranging implications for the use of terahertz in medical imaging. A better understanding of how terahertz interacts with tissue could lead to improvements in technology and analytical techniques.

1.1 *Theory*

Pickwell et al.[13] used a FDTD model, utilizing Maxwell's equations and Debye theory, to describe the propagation of terahertz pulses through water and tissue. For completeness, in this work we outline the fundamental principles of the model and then use it to explain the differences in reflected pulses from carcinoma and normal tissue. References 12, 15, and 16 conclude that in the terahertz regime the response of water can be fitted by a double Debye model characterized by a slow relaxation mode (τ_1) and a fast relaxation mode (τ_2). Debye theory couples the relaxation of the local polarization P to the local electric field E, characterized by time constant τ and coupling strength γ:

$$P + \tau \frac{dP}{dt} = \gamma E. \tag{1}$$

Here, for the first time we use double Debye theory to model BCC following the assumptions in Ref. 14. For a material obeying the double Debye model, the frequency-dependent dielectric function $\hat{\epsilon}(\omega)$ is given by:

$$\hat{\epsilon}(\omega) = \varepsilon_\infty + \frac{\varepsilon_s - \varepsilon_2}{1 + i\omega\tau_1} + \frac{\varepsilon_2 - \varepsilon_\infty}{1 + i\omega\tau_2}, \tag{2}$$

where ε_s is the static dielectric constant, ε_∞ is the limiting value at high frequency, and ε_2 is an intermediate frequency limit. We refer to ε_s, ε_2, ε_∞, τ_1, and τ_2 as the double Debye parameters. The complex dielectric coefficient $\hat{\epsilon}(\omega)$ is related to the complex refractive index $\hat{n}(\omega)$ squared, as in Eq. (3), which shows how the Debye parameters in Eq. (2) are related to the refractive index and the absorption coefficient, which can be directly measured using terahertz pulsed spectroscopy (TPS).

$$\begin{aligned}\hat{\epsilon}(\omega) &= \hat{n}(\omega)^2 \\ &= n(\omega)^2 - \frac{c^2\alpha(\omega)^2}{4\omega^2} - \frac{c}{\omega} n(\omega)\alpha(\omega) i,\end{aligned} \tag{3}$$

where $\hat{n}(\omega) = n(\omega) - ic\alpha(\omega)/2\omega$, such that $n(\omega)$ is the real refractive index and $\alpha(\omega)$ is the absorption coefficient.

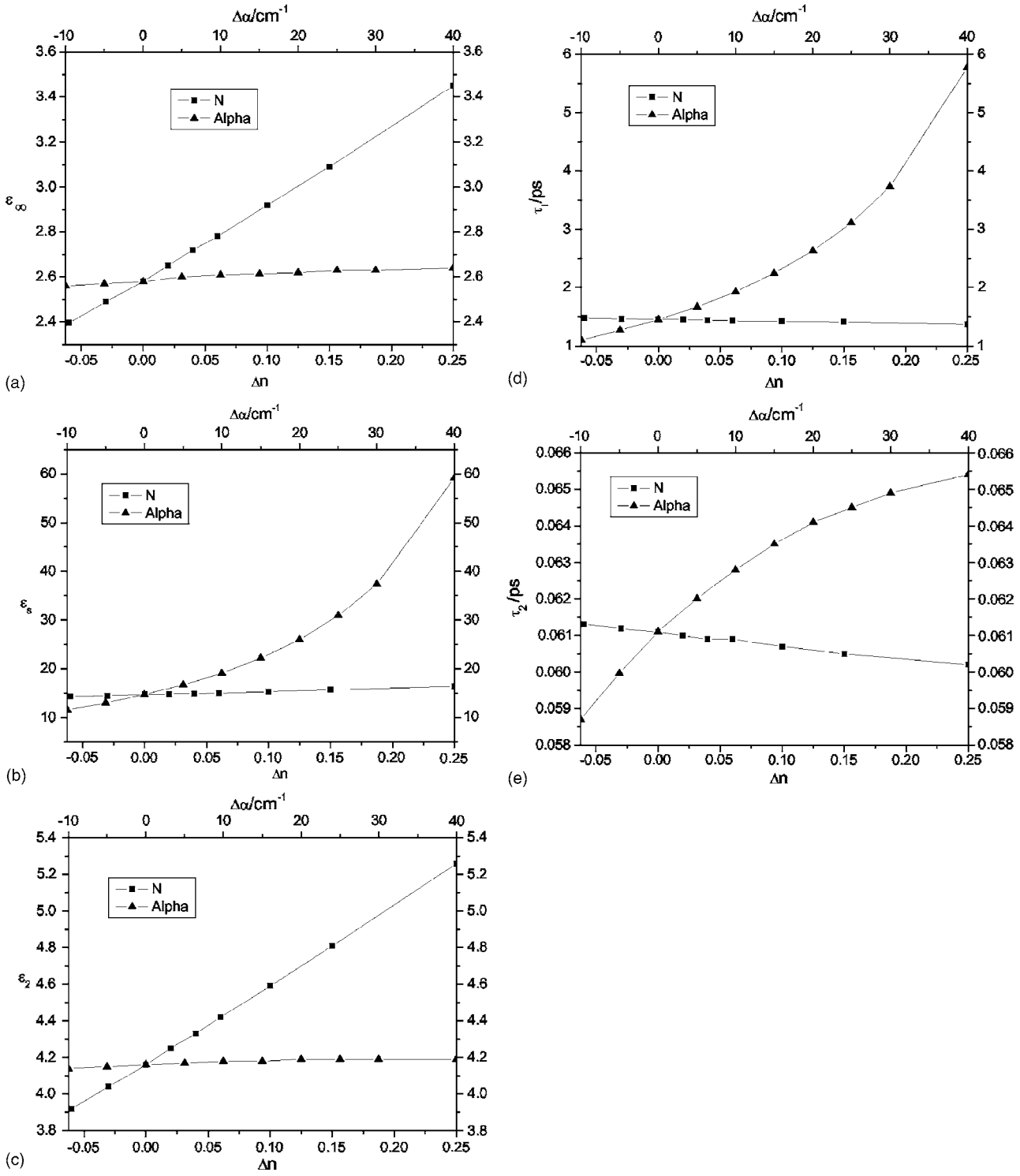

Fig. 2 Dependence on the refractive index and absorption coefficient of the double Debye parameters: (a) ε_∞, (b) ε_s, (c) ε_2, (d) τ_1, and (e) τ_2.

Table 1 Double Debye parameters for *ex vivo* normal tissue and that containing BCC compared to our parameters previously published for *in vivo* normal tissue (epidermis) and water.

	ε_∞	ε_s	ε_2	τ_1/ps	τ_2/ps
Ex vivo normal	2.58	14.7	4.16	1.45	0.0611
Ex vivo BCC	2.65	17.6	4.23	1.55	0.0614
In vivo epidermis[14]	3	58	3.6	9.4	0.18
Water[13]	4.1	78.8	6.6	10.6	0.18

The key concept in the simulation is to incorporate the time dependence of the polarization using double Debye theory in Maxwell's equations (as in Ref. 13). From these equations, we derived iterative equations to model the polarization and the local E and H fields, thus enabling the simulation of the propagation of a terahertz pulse through the discretized region in the time domain. In this work, we study how the double Debye parameters influence the shape of simulated reflected waveforms and which parameters are dominant, and identify reasons for the differences between the waveforms reflected off normal skin tissue and BCC.

2 Materials and Methods

The data used in this study were taken from tissue samples obtained from patients undergoing MMS at the Dermatology Department, Addenbrooke's Hospital, Cambridge, United Kingdom. All ten patients had given their informed and signed consent for surplus skin to be used for research. The samples included BCC and an adjacent piece of normal tissue. These samples were mainly from the head and neck. Spectroscopy measurements of the samples were taken, after which the tissue was returned to Addenbrooke's Hospital for pathologic confirmation.

All spectroscopy measurements were made in transmission using TPI™ Spectra1000 (TeraView Limited, Cambridge, United Kingdom) previously described by Taday and Newnham.[17] Time domain data were obtained in rapid scan mode (30 scans per sec), which when Fourier transformed gave a spectral resolution of 0.03 THz. The spectra contain both phase and amplitude information, hence it is possible to extract the refractive index and absorption coefficient of a sample.

3 Results and Discussion

3.1 *Complex Refractive Index and Double Debye Parameters of Normal Skin and Basal Cell Carcinoma*

We calculated the refractive index and absorption coefficient from the spectral data for normal skin and BCC from the same site by using the mean data from all ten patients. These data are plotted with 95% confidence limits in Fig. 1. From Fig. 1(a) we see that the refractive index n of the tissue containing BCC is higher than the normal tissue throughout the frequency range, and that the difference is more pronounced between 0.25 and 0.75 THz. The absorption coefficient α [Fig. 1(b)] for BCC is also consistently higher than for the normal tissue at 0.5 THz. There is a difference of 16 cm^{-1}, which increases to 25 cm^{-1} at 2 THz. Using this data in the model, the Debye parameters were extracted and are given in Table 1. For comparison, we consider *in vivo* measurements of n and α of tissue from Ref. 14. This was calculated from reflection data from the volar forearm. We find that the n and α calculated from the forearm are much lower than n and α from the normal tissue *ex vivo* data, and thus there are differ-

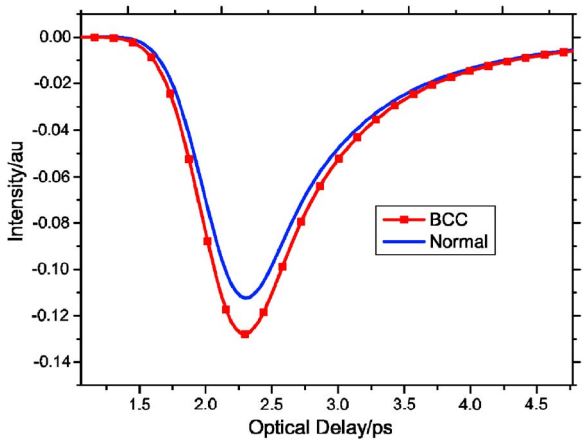

Fig. 3 Simulations of the waveforms reflected off a quartz-tissue interface calculated by using the double Debye parameters extracted from the *ex vivo* normal and BCC tissue data.

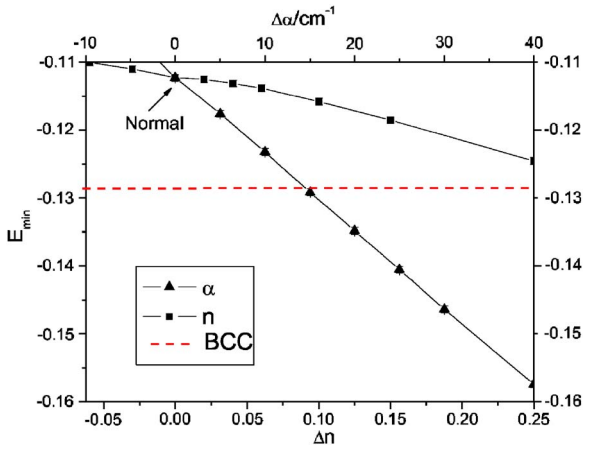

Fig. 4 The dependence of E_{min} on the refractive index and absorption coefficient.

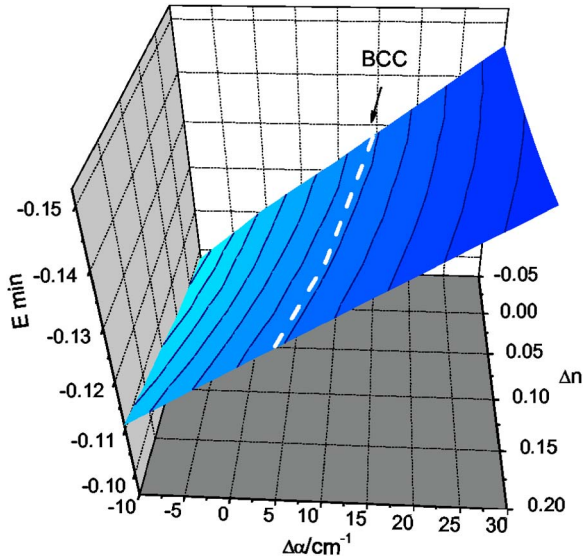

Fig. 5 A 3-D contour plot with isobars of E_{min} as dependent on α and n. The dashed line indicates the isobar of the minimum of the waveform from the simulation of BCC containing tissue.

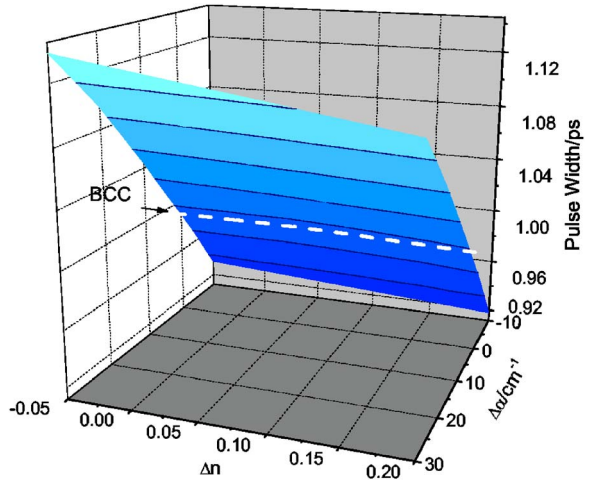

Fig. 6 A 3-D contour plot with isobars of pulse width as dependent on α and n. The dashed line indicates the isobar of the pulse width of the waveform from the simulation of BCC containing tissue.

ences in the Debye parameters given in Table 1. We expect there to be some differences between *in vivo* and *ex vivo* data, because tissue changes after excision, e.g., interstitial fluid, is present around the tissue due to slight compression and body site variation. Due to the differences between *ex* and *in vivo* measurements, we consider the data separately, and it is noted that *ex vivo* spectroscopy gives higher values for n and α when compared to *in vivo* reflection data.

The complex refractive index from the *ex vivo* data between 0.2 and 2 THz was fitted to the frequency-dependent expression for the complex dielectric coefficient in Eq. (2), and the double Debye parameters for the normal tissue and the BCC were extracted. These parameters are given in Table 1, alongside our parameters for *in vivo* normal tissue (epidermis) and water.

The double Debye parameters are dependent on the complex permittivity which, in turn, is dependent on n and α. By changing n and α separately, we look at how the double Debye parameters affect the corresponding waveform properties. We have changed n for normal tissue from −0.06 and 0.25 in steps of 0.01 while keeping α fixed. Then we changed α from −10 and 40 cm^{-1} at intervals of 10 cm^{-1} while keeping n fixed. For each new complex refractive index, the double Debye parameters were calculated. The resulting graphs are illustrated in Figs. 2(a)–2(e).

Figure 2(a) shows that ε_∞ is more dependent on n than α. This is expected, as ε_∞ is the high frequency limit of the dielectric constant, and n converges as the frequency increases. Therefore, increasing n causes an increase in ε_∞. Increasing α also increases ε_∞, although to a lesser extent. This is because the imaginary part of the complex dielectric coefficient falls to zero at the high frequency limit. Conversely, the low frequency limit parameter ε_s is more dependent on changes in α than n, because at low frequencies terms containing α dominate [Eq. (3)]. It is interesting to observe that ε_2 is more sensitive to changes in n than α over this frequency range. This suggests that the intermediate frequency limit corresponds to nearer the higher frequencies rather than the lower. As expected, both the relaxation times τ_1 and τ_2 are more sensitive to α than n. Increasing α increases the relaxation times, which means that reorientation processes are slowing down. In tissue, this could be due to the increased presence of structural proteins to which more water molecules are bound. Thus, a material with higher attenuation will have more bound water molecules which, in this case, hinders the propagation of terahertz radiation and will broaden waves passing through.

3.2 *Simulations of the Interaction of Terahertz Radiation with Basal Cell Carcinoma*

The *ex vivo* parameters in Table 1 were entered into the FDTD model to simulate the reflection off a quartz-tissue interface. This was captured for both the normal and BCC tissue. The quartz-tissue interface is modeled, because *in vivo* images of skin cancer are taken by placement on a z-cut quartz imaging plate, as quartz has a similar refractive index to tissue. Figure

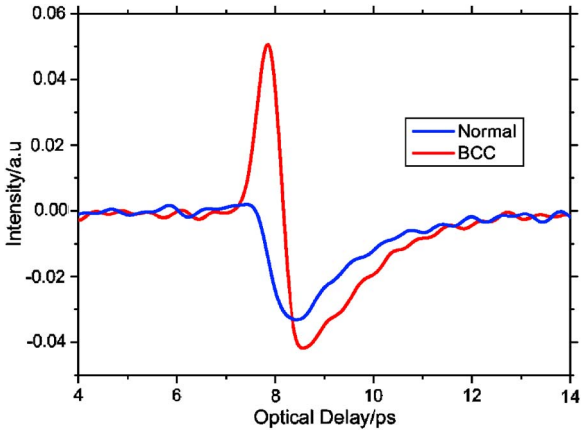

Fig. 7 Waveforms of normal and diseased tissue taken from the terahertz image in Fig. 4 of Ref. 7.

Table 2 Double Debye parameters for normal tissue and that containing BCC as fitted to the *in vivo* image of skin cancer.

	ε_∞	ε_s	ε_2	τ_1 / ps	τ_2 / ps
Simulated *in vivo* normal	3.4	25	5.0	7.0	1.0
Simulated *in vivo* BCC	4.2	40	6.2	10	1.0

3 depicts reflected waveforms and we see that the wave reflected off the tissue containing BCC has a lower minimum (i.e., it is more greatly reflected) than the reflection off the normal tissue. It is a minimum, because the reflection from a quartz-tissue interface has the opposite phase to the reflection from the quartz-air interface (which was used as the reference). The pulse width is the same for both waves. *NB*, the pulse width, is calculated for the time-domain waveform in the same way as the full-width half maximum (FWHM), although here it is the minimum. The combined terahertz properties of the quartz window and the tissue give rise to the shape of the reflected waveform. For example, the difference between the refractive index of the quartz and tissue affects the intensity and phase of the reflected pulse. Therefore, we consider how the reflected amplitude $E_{\min}$ and the pulse width change in simulations using the Debye parameters plotted in Fig. 2 from the systematic changes to n and α. From Fig. 4, we see that increasing both α and n increases the intensity of the reflected waveform, i.e., $E_{\min}$ becomes more negative. Now we consider the effects on $E_{\min}$ and the pulse width when changing α and n together. The results are illustrated in the 3-D contour plots in Fig. 5. Similarly, the effects of changing both α and n on the pulse width are illustrated in Fig. 6. The surface in Fig. 5 illustrates how increasing α and n increase $E_{\min}$. The contour corresponding to the $E_{\min}$ of the wave reflected off BCC is marked where it intersects the surface. This emphasizes the point that by increasing the components of the complex refractive index of normal tissue, we can cause observable changes in the reflected waveform to match those off tissue containing BCC. Similarly in Fig. 6, the contour corresponding to the pulse width of the wave reflected off BCC is marked on the surface, and thus depicts the locus of values of α and n that would provide suitable waveforms. Clearly, the intersection of the loci of α and n from Figs. 5 and 6 will correspond to the deviation of α and n of BCC from normal tissue. Therefore, it may be possible to solve inverse problems and deduce optical properties of tissues from measured reflected waveforms.

4 *In Vivo* Image Data of Basal Cell Carcinoma

We have extracted normal and BCC waveforms from *in vivo* terahertz images previously published in the *British Journal of Dermatology*.[7] These waveforms are depicted in Fig. 7. We then simulated the waveform reflected off the normal tissue using a one-layer system. The BCC was modeled as a two-layer system; a top dry, encrusted area was modeled as a 30-μm region of constant n (ε_∞=3). This was lower than that for quartz to maintain the phase of the wave. The parameters used for the regions of tissue are given in Table 2. The waveforms simulated from these parameters are illustrated in Fig. 8. The simulation of the normal waveform fits the measured data well. The slight peak before the main trough is due to the effect of high frequency components. This is because n for the normal tissue falls significantly below n for quartz (2.12) at higher frequencies (Fig. 1), and waves reflected due to propagating into a medium of lower n have opposite phase to those entering a medium of higher n. The simulation of the BCC waveform has the same overall features as the measured waveform. The main difference is the peak height representing the surface reflection, but since it is the layer below that we are most interested in, this is not problematic. The most significant differences between the *ex vivo* parameters for normal and BCC tissue were in ε_∞, ε_s, and τ_1. This is also the

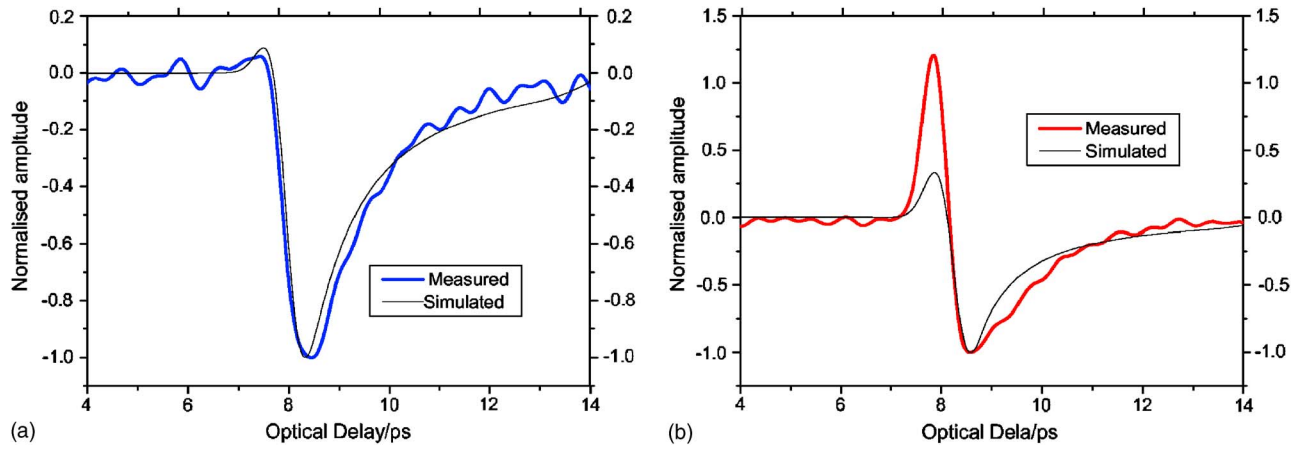

Fig. 8 Simulations of (a) healthy tissue and (b) tissue containing BCC compared with respective pixels from an *in vivo* image of skin cancer.

case for the parameters used to simulate the normal and BCC waveforms in the *in vivo* data, and the trends are the same. We then calculated the respective n and α for the tissues from the *in vivo* double Debye parameters. As expected, there were differences between *ex vivo* and *in vivo* results for the complex refractive index of tissue. However, due to the changes in tissue caused by excision, such as tissue shrinkage and leaking of interstitial fluids, it is not so meaningful to compare *ex vivo* results with *in vivo* results. Therefore, we just consider the relative differences between normal and diseased tissue from the *in vivo* data.

We calculated n and α from the *in vivo* simulation parameters and observed that n and α for BCC are consistently higher than for the normal tissue. This corroborates the *ex vivo* complex refractive index measurements, and suggests that *in vivo* BCC also has a higher n and α than normal *in vivo* tissue. This is also consistent with the notion that tumor has a higher water content than normal tissue, as n and α for the BCC are closer to n and α for water than the normal tissue. Once the complex refractive index of tissue is known, then the optical delay axis of image data can be converted to distance, thus giving information about the depth of the tumor. However, this would require an extensive clinical study to confirm the correlation of measured tumor depth with true tumor depth.

5 Conclusions

We find by using TPS that the refractive index and absorption coefficient of excised tissue containing BCC are both higher than those of normal tissue. We use these data to simulate the propagation of terahertz radiation through diseased and healthy tissue and compare it with *in vivo* reflection data. We find good agreement of the model with real data, but with some discrepencies, which can be explained by the difference between *ex vivo* and *in vivo* measurements.

Acknowledgments

We thank Beverley Haynes at Addenbrooke's Hospital for preparation of the histology slides. Emma Pickwell gratefully acknowledges financial support from Engineering and Physical Sciences Research Council and TeraView Limited.

References

1. C. J. Strachan, P. F. Taday, and D. A. Newnham, "Terahertz pulsed spectroscopy to quantify pharmaceutical polymorphism and crystallinity," *J. Pharm. Sci.* **94**(4), 837–846 (2005).
2. C. Baker, W. R. Tribe, B. E. Cole, and M. K. Kemp, "Developments in people-screening using terahertz technology," *Proc. SPIE* **5616**, 61–68 (2004).
3. A. J. Fitzgerald, E. Berry, N. N. Zinov'er, S. Homer-Vanniasinkam, R. E. Miles, M. Chamberlain, and M. A. Smith, "Catalogue of human tissue optical properties at terahertz frequencies," *J. Biol. Phys.* **129**, 123–128 (2003).
4. V. P. Wallace, P. F. Taday, A. J. Fitzgerald, R. M. Woodward, J. Cluff, and D. D. Arnone, "Terahertz pulsed imaging and spectroscopy for biomedical and pharmaceutical applications," *Faraday Discuss.* **126**, 255–263 (2003).
5. E. Berry, G. C. Walker, A. J. Fitzgerald, N. N. Zinov'er, M. Chamberlain, S. W. Smye, R. E. Miles, and M. A. Smith, "Do *in vivo* terahertz imaging systems comply with safety guidelines?" *J. Laser Appl.* **15**(3), 192–198 (2003).
6. R. M. Woodward, V. P. Wallace, R. J. Pye, B. E. Cole, D. D. Arnone, E. Linfield, and M. Pepper, "Terahertz pulsed imaging for *ex vivo* basal cell carcinoma," *J. Invest. Dermatol.* **120**, 72–78 (2003).
7. V. P. Wallace, A. J. Fitzgerald, S. Shankar, N. Flanagan, R. J. Pye, J. Cluff, and D. D. Arnone, "Terahertz pulsed imaging of basal cell carcinoma *ex vivo* and *in vivo*," *Br. J. Dermatol.* **151**, 424–432 (2004).
8. M. Bruehlmeier, U. Roelcke, P. Blauenstein, J. Missimer, P. A. Schubiger, J. T. Locher, R. Pellikka, and S. M. Ametamey, "Measurement of the extracellular space in brain tumors using 76br-bromide and PET," *Eur. J. Nucl. Med.* **44**, 1210–1218 (2003).
9. K. F. Ross and R. E. Gordon, "Water in malignant tissue, measured by cell refractometry and nuclear magnetic resonance," *J. Microsc.* **128**, 7–21 (1982).
10. J. H. Chen, H. E. Avram, L. E. Crooks, M. Arakawa, L. Kaufman, and A. C. Briton, "*In vivo* relaxation times and hydrogen density at 0.063–4.85 t in rats with implanted mammary adenocarcinomas," *Radiology* **184**, 427–434 (1992).
11. E. K. Rofstad, E. Steinsland, O Kaalhus, Y. B. Chang, B. Hovik, and H. Lyng, "Magnetic resonance imaging of human melonoma xenografts *in vivo*: Proton spin lattice and spin-spin relaxation times versus fractional water content and fraction of necrotic tissue," *Int. J. Radiat. Biol.* **65**, 387–401 (1994).
12. C. Ronne and S. R. Keiding, "Low frequency spectroscopy of liquid water using THz-time domain spectroscopy," *J. Mol. Liq.* **101**(1–3), 199–218 (2002).
13. E. Pickwell, B. E. Cole, A. J. Fitzgerald, M. Pepper, and V. P. Wallace, "Simulation of terahertz pulse propagation in biological systems," *Appl. Phys. Lett.* **84**(12), 2190–2192 (2004).
14. E. Pickwell, B. E. Cole, A. J. Fitzgerald, M. Pepper, and V. P. Wallace, "*In vivo* study of human skin using pulsed terahertz radiation," *Phys. Med. Biol.* **49**, 1595–1607 (2004).
15. J. T. Kindt and C. A. Schmuttenmaer, "Far infrared dielectric properties of polar liquids probed by femtosecond terahertz pulse spectroscopy," *J. Phys. Chem.* **100**, 10373–10379 (1996).
16. C. Ronne, L. Thrane, P. Astrand, A. Wallqvist, K. V. Mikkelsen, and S. R. Keiding, "Investigation of the temperature dependence of dielectric relaxation in liquid water by THz reflection spectroscopy and molecular dynamics simulation," *J. Chem. Phys.* **107**, 14 (1997).
17. P. F. Taday and D. A. Newnham, "Technological advances in terahertz pulsed systems bring far-infrared spectroscopy into the spotlight," *Spectroscopy Europe* pp. 20–24 (2004).